Raman Surface Vibration Modes in Nanocrystalline SnO_2: Correlation with Gas Sensor Performances

Marina N. Rumyantseva,[†] Alexander M. Gaskov,[†] N. Rosman,[‡] T. Pagnier,[‡] and Juan R. Morante*[,§]

Chemistry Department, Moscow State University, Leninskie Gory, Moscow, 119992 Russia, LEPMI-ENSEEG, 1130, rue de la Piscine, BP 75, Saint Martin d'Hères, 38402 France, and Electronic Materials and Engineering, EME/CeRMAE, Department of Electronics, Physics Faculty, University of Barcelona, C/Martí I Franquès 1, Barcelona, 08028 Spain

Received June 15, 2004. Revised Manuscript Received October 26, 2004

Raman surface vibration modes have been measured for SnO_2 nanocrystalline powders with grain sizes of 3−36 nm and a specific surface area up to 180 $m^2\ g^{-1}$, which were prepared by four different routes of chemical synthesis. The influence on these surface vibration modes of the treatment temperature, the crystallite size, and the specific surface area has been studied and bands at 245, 257, 286, 310−350, and 400−700 cm^{-1} have been identified. The 400−700 cm^{-1} band intensity has been found proportional to the surface active area. Likewise, the correlation of the 400−700 cm^{-1} band intensity with the sensing mechanisms have been analyzed from the sensor response of the prepared thick-film gas sensors against reducing CO and oxidizing NO_2 species diluted in a N_2 carrier. The influence of the nanostructure surface on the sensor signal exhibits opposite trends for CO than for NO_2 detection. As the Raman surface vibration modes, 400−700 cm^{-1}, band intensity increases, the sensor response for CO increases too, while that of NO_2 diminishes, giving an excellent inverse correlation between the sensor response for CO and NO_2. This correlation is fulfilled for all the samples except those that are distorted by the presence of an excess of contamination caused by OH^- groups together with Cl^- ions introduced by the chemical synthesis procedure.

Introduction

Despite the simple basic idea of the gas detection principle using semiconductor metal oxide, the involved mechanisms in the gas sensing processes are rather complex. They are related mainly with several steps such as gas adsorption, chemical reactions taking place at the grain surface, and charge transport. All these processes depend on material structure, which is usually referenced by the grain size only.[1,3] In this framework, it is frequently claimed that nanometer-scaled materials have significant advantages because of their small grain size, which becomes important to increase the adsorption capacity of these materials, but there are only a few works considering the influence of specific surface area on gas sensor properties.[4,5] However, there is different experimental evidence suggesting that the peculiarities of structure and surface composition of nanocrystalline systems derived from synthesis conditions are behind the discrepancies among the functional properties of these materials. So, in a previous work devoted to the influence of calcination procedure on the response of the nano-SnO_2 based sensor,[6] the hypothesis was already pointed out that the improved NO_2 response with respect to that of the CO could be attributed to a more important role played by the surface characteristics than the grain size modification itself.

In this work, to analyze the nanostructure surface influence on the sensing mechanisms, we have used four synthesis techniques to obtain different nanocrystalline oxide powders with grain sizes from 3 to 36 nm and specific surface values of more than 100 $m^2\ g^{-1}$. Then, we have determined and studied the evolution of Raman surface vibration modes as a powerful tool to reveal straightforwardly the surface characteristics of these nanocrystalline powders which determine the surface reactivity with the target specimens. The NO_2 and CO gas response of these nanomaterials has also been analyzed. Finally, the relationships between nanostructure surface, determined by the Raman band intensity, and the gas response are reported and discussed, corroborating the significant role played by the surface characteristics.

Experimental Section

Powders of tin dioxide have been elaborated by four different modifications of wet chemical synthesis indicated as g, k, h, and s as shown in Figure 1. SnO_2 powder g was prepared by conventional

* To whom the correspondence should be addressed. E-mail: morante@el.ub.es. Phone/Fax: +34934021140/48.
[†] Moscow State University.
[‡] LEPMI-ENSEEG.
[§] University of Barcelona.

(1) Xu, C.; Tamaki, J.; Miura, N.; Yamazoe, N. *Sens. Actuators, B* **1991**, *3*, 147−155.
(2) Barsân, N. *Sens. Actuators, B* **1994**, *17*, 241−246.
(3) Barsân, N.; Schweizer-Berberich, M.; Göpel, W. *Fresenius J. Anal. Chem.* **1999**, *365*, 287−304.
(4) Li, G. J.; Kawi, S. *Talanta* **1998**, *45*, 759−766.
(5) Li, G. J.; Chang, X. H.; Kawi, S. *Sens. Actuators, B* **1999**, *60*, 64−70.
(6) Dieguez, A.; Romano-Rodriguez, A.; Morante, J. R.; Kappler, J.; Barsan, N.; Gopel, W. *Sens. Actuators, B* **1999**, *60*, 125−137.

10.1021/cm0490470 CCC: $30.25
Published on Web 01/29/2005

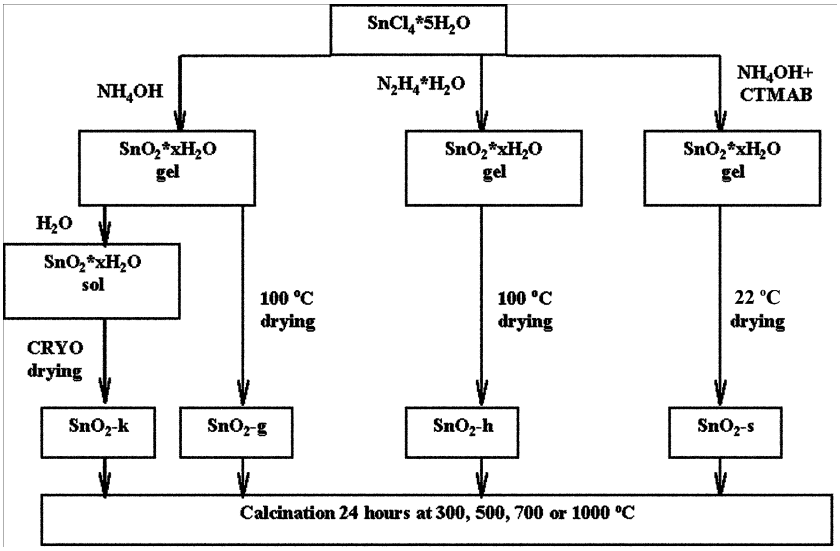

Figure 1. Scheme of the used synthesis methods for SnO_2 powders.

hydrolysis of $SnCl_4$. A measured amount of $SnCl_4 \cdot 5H_2O$ was dissolved in deionized water in an ice bath, and liquid ammonia was slowly added to the stirred solution to achieve a complete precipitation of α-stannic acid. The resulting gel was centrifuged, washed with deionized water to complete disappearance of the chloride ions ($AgNO_3$ test), and dried at 100 °C during 24 h.

Sample k was elaborated by means of the cryosol technique.[7] The stable sol of α-stannic acid was obtained from the corresponding gel as a result of electrolyte (NH_4Cl) elimination during washing with deionized water.[8] The powder was obtained by freeze-drying of sol in a sublimator (SMH-15, Usifroid) after pulverization in liquid nitrogen.

Series h was prepared by the method described in ref 9. The hydrolysis of $SnCl_4$ was realized using an aqueous solution of hydrazine monohydrate, $N_2H_4 \cdot H_2O$. A white precipitate was formed at room temperature and maintained under stirring at reflux for 3 days. As for the g samples the precipitate was submitted to a centrifugation−washing sequence until the absence of chloride ion. The resulting gel was dried at 100 °C during 24 h.

SnO_2 powder s was synthesized starting from $SnCl_4 \cdot 5H_2O$ and NH_4OH with use of cationic surfactant cetyltrimethylammonium bromide (CTAB) as the organic supramolecular template.[10] First the NH_4OH solution was added into CTAB aqueous solution under stirring until the mixture became homogeneous. Then the aqueous solution of $SnCl_4 \cdot 5H_2O$ was introduced into the mixture producing a white sol. After stirring for 5 h the product was aged at room temperature for 72 h. The resulting gel was centrifuged, washed with deionized water, and dried at room temperature.

All dried powders were crushed and calcined in the same conditions: in air at 300, 500, 700, and 1000 °C during 24 h. The sample characteristics are presented in Table 1.

Different techniques were applied to determine the composition, morphology, structure, and electrical properties of the samples. The analysis of Cl content in annealed samples was done by laser-induced mass spectrometry using the EMAL-2 setup.

Table 1. Characteristics of SnO_2 Samples Prepared by Different Routes

sample	annealing temp, °C	Cl content, at. %	SnO_2 av grain size, d_{XRD}, nm	specific surface area, S_{surf}, m^2g^{-1}
g300	300		4	122
g500	500	1.0	9	35
g700	700		22	9
g1000	1000		35	
k300	300	2.8	4	175
k500	500	1.4	9	65
k700	700	0.04	17	28
k1000	1000		26	
h300	300		4	135
h500	500	5.1	11	26
h700	700		34	12
h1000	1000		35	
s300	300		3	180
s500	500		11	69
s700	700		22	14
s1000	1000		36	

Thermogravimetric analysis (TGA) was performed using the DSC-7 (Perkin-Elmer) technique. The samples were heated in air from room temperature up to 1000 °C with a heating rate of 10 °C min^{-1}.

X-ray diffraction (XRD) patterns were recorded using a STOE diffractometer with monochromatic Cu Kα radiation. The results were processed using STOE WinXPow software. The SnO_2 average grain size (d_{XRD}) was estimated from the XRD data using the Debye−Scherrer equation applied to the most intense 110 and 101 diffraction lines.

Transmission electron microscopy (TEM) was carried out on a Phillips CM30 SuperTwin electron microscope operated at 300 keV with 0.19-nm point resolution. For TEM observations, SnO_2 nanopowders were ultrasonically dispersed in ethanol and deposited on amorphous holey carbon membranes.

Specific surface area value of tin dioxide samples was calculated from measurements of N_2 adsorption−desorption isotherms. The linear portion of the BET plot was used taking the data below $P/P_0 = 0.3$. Prior to the measurements all samples were treated under vacuum at 200 °C for 2 h.

Raman spectra were collected using a DILOR XY spectrometer equipped with a cooled CCD detector. The green line of an Ar laser (514.53 nm) in micro-Raman configuration (objective 50×) was used. All spectra were recorded at room temperature in air.

(7) Kudryavtseva, S. M.; Vertegel, A. A.; Kalinin, S. V.; Oleynikov, N. N.; Ryabova, L. I.; Meshkov, L. L.; Nesterenko, S. N.; Rumyantseva, M. N.; Gaskov, A. M. *J. Mater. Chem.* **1997**, *7*, 2269−2272.
(8) Sonntag, H.; Strenge, K. *Koagulation und stabilität disperser systeme;* VEB Deutcher Verlag der Wissenschaften, Berlin, 1970; p 30.
(9) Sergent, N.; Gelin, P.; Perier-Camby, L.; Praliaud, H.; Thomas, G. *Sens. Actuators, B* **2002**, *84*, 176−188.
(10) Wang, Yu. D.; Ma, Ch. L.; Sun, X. D.; Li, H. D. *Mater. Lett.* **2001**, *51*, 285−288.

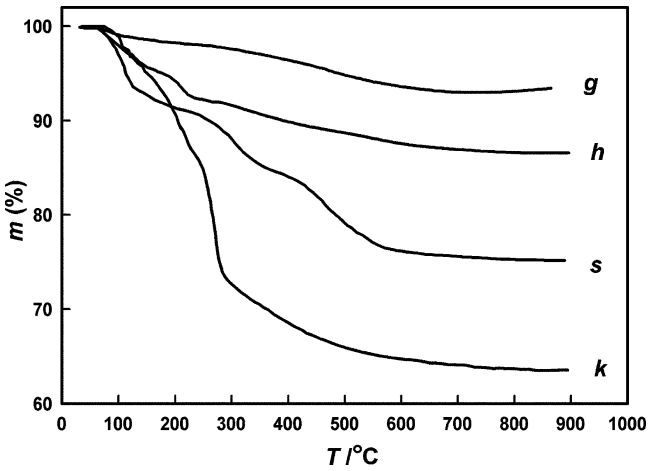

Figure 2. TGA (mass loss) curves for samples prepared by various routes.

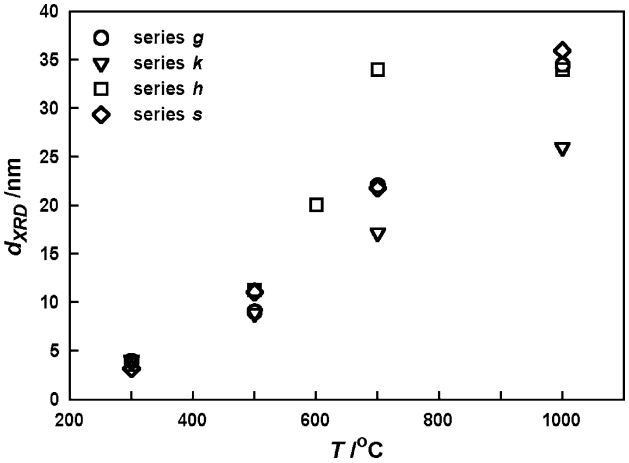

Figure 3. Average grain diameter of SnO_2 crystallites (d_{XRD}) against calcination temperature for various synthesis methods.

FTIR transmission spectra were recorded from 400 to 4000 cm^{-1} with a resolution of 4 cm^{-1} using a Perkin-Elmer-1600 spectrometer at room temperature. Sample pellets containing 200 mg of KBr and 2 mg of SnO_2 were prepared to allow a quantitative comparison of spectra of different samples.

To study the gas sensor properties, thick films were prepared on polycrystalline Al_2O_3 substrates with previously deposited gold contacts. Screen printing technique was used for thick-film deposition starting from the pastes of powders with a terpineol−ethanol mixture. Films were dried at 100 °C for 24 h and calcined at 500 °C for 6 h. Platinum wires were pressed to the gold contacts for signal recording. The measurements of electric current proportional to the conductivity value were performed in dc mode at a fixed voltage $U = 1$ V. The comparison of the conductivity (resistivity) values in dry air G_o (R_o) and in the gas containing atmosphere G (R) allowed the estimation of electrical response $S(CO) = (G - G_o)/G_o$ in relation to the CO concentration or $S(NO_2) = (R - R_o)/R_o$ versus the NO_2 concentration.

Results and Discussion

Figure 2 shows the integral curves of thermogravimetric analysis taken for the samples that were not calcined. Different mass loss behaviors were observed for different preparation methods. Series k exhibits the maximum mass loss value caused by evaporation of water. The presence of significant water concentration is associated with formation of SnO_2 sol within the synthesis procedure. SnO_2 particles in the sol have the smaller dimension as compared with those in the gel. That results in an increase of the amount of H_2O molecules forming a hydrate cover around SnO_2 particles. The mass loss in g and h series are associated with elimination of byproducts NH_4Cl, N_2H_5Cl, $N_2H_4Cl_2$, and water desorption. The significant mass loss value in series s is due to oxidative decomposition of CTAB.

XRD spectra demonstrate that all powders consist of SnO_2 cassiterite phase. Average crystallite diameters were obtained with the Scherrer formula from (110) peaks. As is shown in Figure 3, the average size of SnO_2 crystallites (d_{XRD}) varies from 3 to 36 nm depending on treatment temperature and synthesis method. To analyze the temperature dependence of crystallite size for series h, an additional sample annealed at 600 °C was also prepared; see Figure 3. Series k has the lowest crystallite size in the temperature range 500−1000 °C. This feature found for SnO_2 powders obtained by the cryosol technique has also been observed in ref 7.

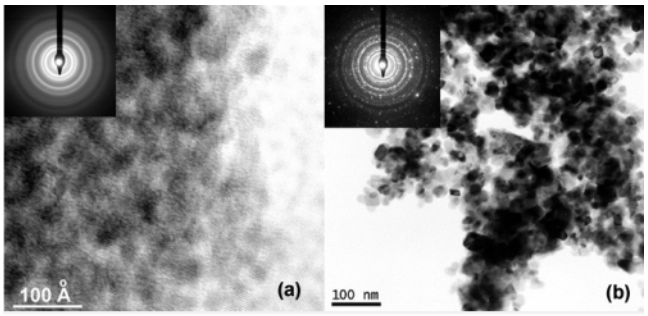

Figure 4. TEM images of samples g300 (a) and g700 (b).

Table 2. Crystallographic Planes in Different SnO_2 Samples

family planes	SnO_2 bulk d (Å)	sample g300 d (Å)	sample g700 d (Å)	sample k700 d (Å)
(110)	3.347	3.379	3.353	3.351
(101)	2.643	2.657	2.653	2.649
(200)	2.369		2.342[a]	2.336[a]
(111)	2.309	2.315	2.342[a]	2.336[a]
(210)	2.119		2.112	2.108
(211)	1.764	1.768	1.771	1.766
(220)	1.675			
(002)	1.593		1.594	1.589
(310)	1.498		1.504	1.501
(112)	1.439	1.433	1.428	

[a] SnO_2 has two families of planes with values very close: (200) with a d spacing of 2.369 Å and (111) with a d spacing of 2.309 Å. For g300 only, appears the family (111), but the samples g700 and k700 both appear, thus producing a problem in fitting algorithm. So, the obtained values in this case are basically just an artifact of the fitting procedure.

To examine the influence of organic vehicle and additional thermal annealing during preparation of thick films on crystallite size, XRD spectra were taken for the powders g300, k300, h300, and s300 mixed with the terpineol−ethanol vehicle and annealed in the same conditions as corresponding thick films. No differences were detected in XRD spectra of as-prepared and treated powders. So, one can conclude that powders and corresponding thick films are characterized by the same size of SnO_2 crystallites.

TEM images of samples g300 and g700 are shown in Figure 4. Sample g300 (Figure 4a) presents a rounded shape, which corresponds still to the energy minimization for particle nucleation. From a crystallographic point of view

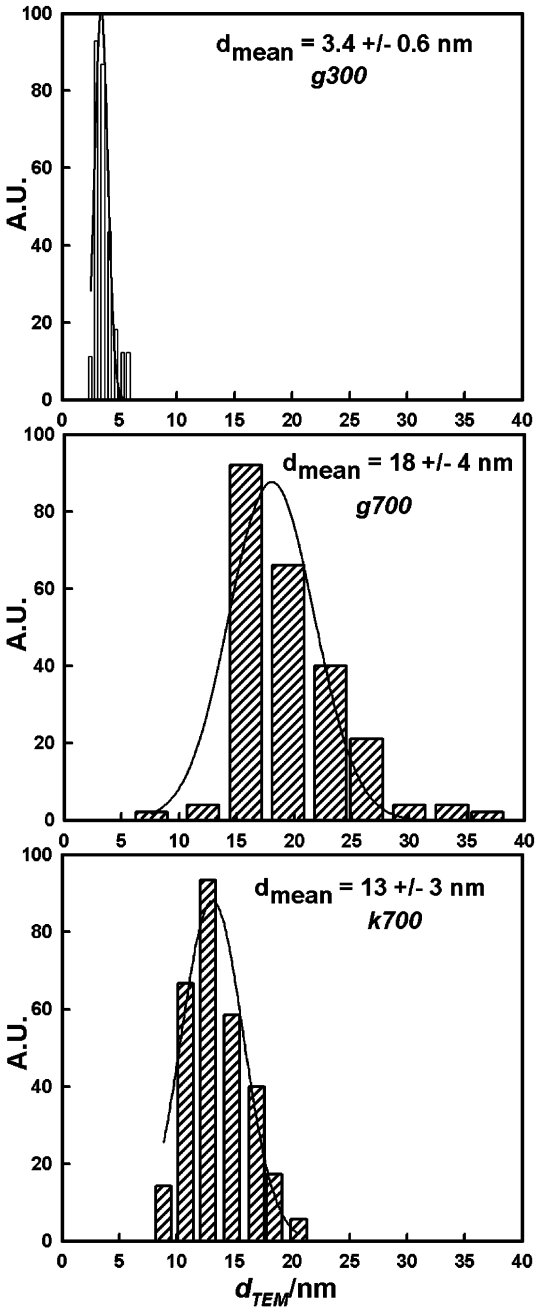

Figure 5. Nanoparticle size distribution extracted from the TEM analysis of g300, g700, and k700 powders.

the lattice is not yet presenting a well-defined surface faceting and the particles have a significant lattice distortion at these finishing layers of the grain. On the contrary, sample g700 (Figure 4b) is already presenting a faceted surface, which corresponds to a much better defined surface of the nanoparticles.

The families of crystallographic planes obtained from electron diffraction data for samples g300, g700, and k700 are collected in Table 2. It should be remarked that for the g300 sample, it was not possible to determine many of its crystallographic characteristics, due to its complex structure and to an important lattice distortion for (110) family of planes.

The histograms of the grain size distributions of the powder are Ze presented in Figure 5. The SnO_2 average grain size d_{TEM} are in agreement with the values estimated for these

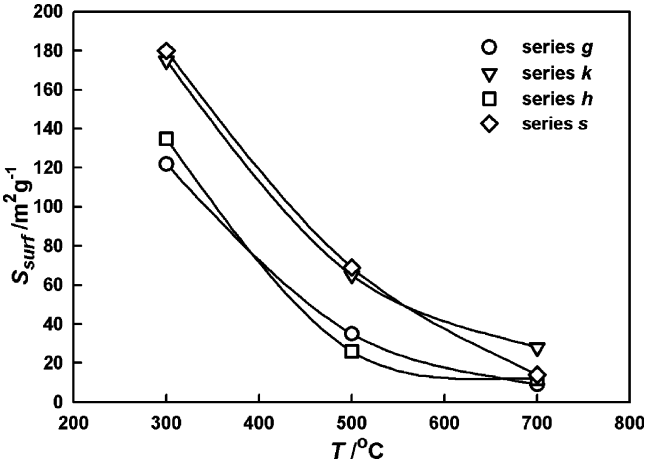

Figure 6. Specific surface area S_{surf} vs calcination temperature depending on synthesis methods.

Table 3. Comparison of SnO_2 Crystallite Size and Agglomeration Degree

sample	d_{XRD}, nm	d_{BET}, nm	d_{BET}/d_{XRD}
g300	4	7	1.8
g500	9	25	2.8
g700	22	96	4.4
k300	4	5	1.3
k500	9	13	1.4
k700	17	31	1.8
h300	4	6	1.5
h500	11	33	3.0
h700	34	72	2.1
s300	3	5	1.7
s500	11	13	1.2
s700	22	62	2.8

samples from XRD spectra (d_{XRD}, Table 1). As expected, the increase of annealing temperature leads to grain growth and broadening of grain size distribution. Nevertheless, it is worth remarking that synthesis method has a strong influence on the grain size evolution in relation with the thermal treatment. Powder prepared using the cryosol technique (sample k700) is characterized by a narrow grain size distribution as compared with sample g700 obtained by conventional hydrolysis and calcined at the same temperature of 700 °C. This fact is in agreement with the thermal stability of series k.[7]

The SnO_2 powders treated at 300 °C are characterized by specific surface area S_{surf} of 120−180 m^2g^{-1}. These values decrease monotonically as annealing temperature increases for all series (Figure 6). This correlates with the grain size variation. It should also be noted that the k and s series show a higher S_{surf} than g and h samples annealed in the same conditions. So, k and s synthesis methods seem to be preferable to obtain SnO_2 materials with high surface area. The size of SnO_2 agglomerates whose surface is really open for gas adsorption can be estimated from S_{surf} values using an approach of spherical particle shape:

$$d_{BET} = \frac{6 \times 1000}{\rho S_{surf}}$$

where d_{BET} (nm) is this equivalent size or BET size and $\rho = 6.95$ g/cm^3 is the SnO_2 density.

The obtained results are presented in Table 3. In all cases $d_{BET} > d_{XRD}$. The agglomeration degree, defined as $d_{BET}/$

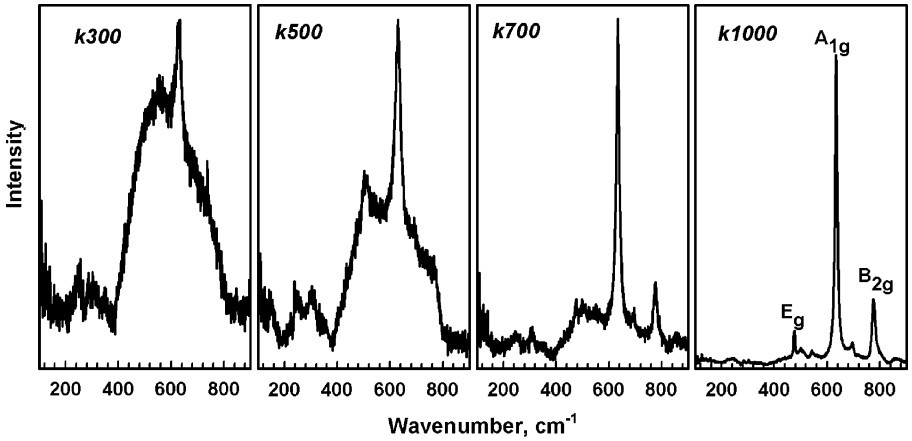

Figure 7. Raman spectrum evolution with the calcination temperature for k series.

d_{XRD}, depends on synthesis method and annealing temperature. Samples of k series exhibit the minimum agglomeration degree as well as a minimum grain size.

Figure 7 shows the evolution of Raman spectra versus the treatment temperature T_c for k series. The spectrum of well-crystallized k1000 sample, grain size 26 nm, is similar to that of microcrystalline SnO_2. The three detectable Raman active modes of tin oxide have been observed: E_g (476 cm^{-1}), A_{1g} (629 cm^{-1}), and B_{2g} (772 cm^{-1}). Spectra of k300, k500, and k700 samples exhibit also around the A_{1g} mode a broad feature attributed to surface modes.[11,12] In addition, bands, which, as far we know, never have been reported, appear in the 310-350 cm^{-1} region. These bands appear as a single broad feature composed of at least two components in the powders heat-treated at 300 °C. For powders treated at higher temperatures, three other bands are observed at 245, 257, and 286 cm^{-1}, together with the broad feature located at the region 310−350 cm^{-1}, which has lost most of its intensity. The Raman spectrum of thick films, which have been treated at 500 °C during 6 h to remove the organic vehicle of the prepared pastes, show only the bands at 245, 257, and 286 cm^{-1} (Figure 8) and no signal in the region 310−350 cm^{-1}, which is only found at low-temperature treated materials. In all cases, these bands disappear for samples heat-treated at 1000 °C. The origin of these bands is not yet elucidated. Liu et al.[13] have reported, besides the expected E_g and A_{1g} bands, Raman bands located at 216,49 and 232,92 cm^{-1} in rutile SnO_2 nanorods, which were attributed to E_u (TO) and E_u (LO) active modes. On the contrary, Hu et al.,[14] working in similar SnO_2 nanoribbons, have only pointed out the existence of a considerable shift, ∼10 cm^{-1}, in the nanoribbons Raman spectra, which present only narrow peaks located at 425 (A_{2g}), 462 (E_g), 620 (A_{1g}), and 762 cm^{-1} (B_{2g}), whereas Zheng et al.[15] pointed out the modes A_{1g} and B_{2g} in SnO_2 nanowires synthesized inside of anodic alumina membrane. A more detailed analysis of these spectra obtained in these nanostructured SnO_2 materials also suggests the presence of the 310−350 cm^{-1} band although it was not discussed by the authors. On the contrary, other authors[16] associated the appearance of a 327 cm^{-1} centered band to the forced hydrolysis of $SnCl_4$ solutions although other ones propose that this band is related to the surface defects[17] or the SnO_2 nanocluster formation, which might constitute a new kind of vibration mode.[18] It is well known that some inactive modes in bulk material can be active because of the size effect in very small particles or in nanostructures with some reduced dimension. So, it is plausible to take into account that this band could be due to an active mode from the inactive E_u mode.[11,12] Nevertheless, more work is still needed to clarify the origin of this band in very tiny SnO_2 structures that, recently, has also been found in the Raman spectra of nanobelts[19] obtained by thermal evaporation of Sn powders. It seems to strengthen

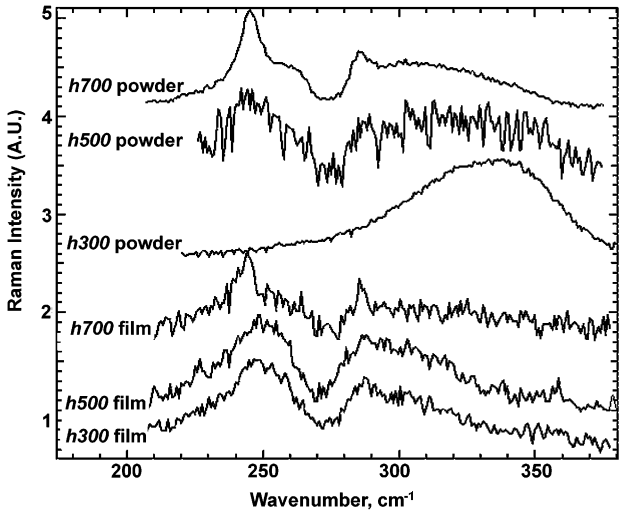

Figure 8. Low-frequency Raman spectra of powders and thick films for h series.

(11) Abello, L.; Bochu, B.; Gaskov, A.; Koudryavtseva, S.; Lucazeau, G.; Rumyantseva, M. *J. Solid State Chem.* **1998**, *135*, 78−85.
(12) Diéguez, A.; Romano- Rodrìguez, A.; Vila, A.; Morante, J. R. *J. Appl. Phys.* **2001**, *90*, 1550−1557.
(13) Liu, Y.; Zheng, C.; Wang, W.; Yin, C.; Wang, G. *Adv. Mater.* **2001**, *13*, 1883−1886.
(14) Hu, J. Q.; Ma, X. L.; Shang, N. G.; Xie, Z. Y.; Wong, W. B.; Lee, C. S.; Lee, S. T. *J. Phys. Chem. B* **2002**, *106*, 3823−3826.
(15) Zheng, M.; Li., G.; Zhang, X.; Huang, S.; Lei, Y.; Zhang, L. *Chem. Mater.* **2001**, *13*, 3859−3861.
(16) Ristic, M.; Ivanda, M.; Popovic, S.; Music, S. *J. Non-Cryst. Solids* **2002**, *303*, 270−280.
(17) Ocaña, M.; Serna, C. J.; Garcia-Ramos, J. V.; Matijevic, E. *Solid State Ionics* **1993**, *63*−*65*, 170.
(18) Yu, K. N.; Xiong, Y.; Liu, Y.; Xiong, C. *Phys. Rev. B* **1997**, *55*, 2666−2671.
(19) Sun, S. H.; Meng, G. W.; Zhang, G. X.; Gao, T.; Geng, B. Y.; Zhang, L. D.; Zuo, J. *Chem. Phys. Lett.* **2003**, *376*, 103−107

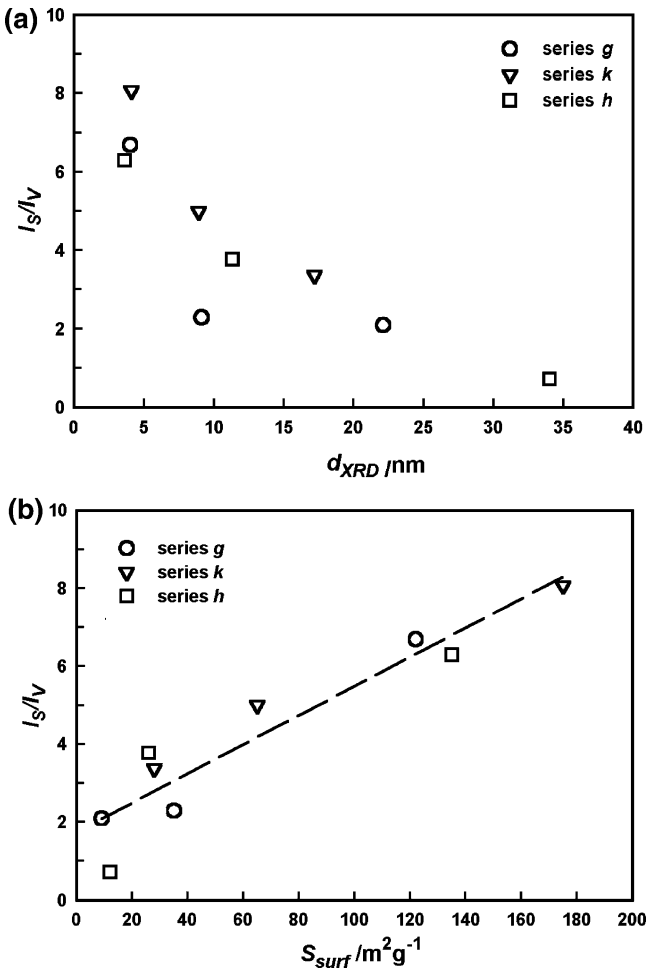

Figure 9. Raman relative intensity of surface modes I_S/I_V value vs SnO_2 crystallite size d_{XRD} (a) and specific surface area S_{surf} (b).

the association of this band with the effects due to the nanostructure size against those due to the synthesis procedure.

The other peculiarity of Raman spectra of nanocrystalline SnO_2 is the very broad feature between 400 and 700 cm^{-1}, now called band of the surface modes. In this region also appear the volume modes (i.e., those appearing in large crystals) of SnO_2. The origin of these bands has been connected to the low particle dimension of the materials. In a previous work,[11] some of us attempted to connect the bands to Raman forbidden and/or corner zone modes becoming active because of the loss of long-range periodicity in nanocrystals. Alternately, Diéguez et al.[12] proposed that surface modes were due to the existence of a lattice softening taking place in the outer part of the grain, which is like a disordered lattice skin around each grain. On the other hand, studies of nanocrystalline tin oxide reactivity versus H_2S have shown that the relative intensity of surface bands depends strongly on the interactions with gases,[20,21] which can modify the outer layers of the grain. So, to analyze these performances at the present cases, the relative intensity of surface modes have been taken as the ratio of the sum of their intensities I_S to the intensity of A_{1g} mode I_V. These intensities are calculated by fitting A_{1g} mode and the B_{2g} mode when needed with Lorentzian-shaped peaks, and the surface modes with five large Gaussian peaks with Peakfit software. I_V was taken as the area of the Lorentzian A_{1g} peak, while I_S was the sum of the five Gaussian peak areas.

Table 4. Sensor Response of SnO_2 Thick Films toward N_2 $S(N_2)$, 900 ppm CO/N_2 $S(CO)$, and 90 ppm NO_2/N_2 $S(NO_2)$

sample	$S(N_2)$	$S(CO)$	$S(NO_2)$
g300	3.7	23	15
g500		12	60
g700		8	110
g1000			130
k300	2.8	26	168
k500		15	190
k700		18	77
h300	2.8	23	14
h500	3.4	19	25
h700	2.4	7	48
s300			53
s500			41
s700			130

The variations of I_S/I_V value versus SnO_2 crystallite size d_{XRD} and specific surface area S_{surf} for g, k, and h series films are presented in Figure 9. The following features should be noted: (i) There is a monotonic diminution of the surface modes as the grain size d_{XRD} increases, which confirms a general trend. (ii) There is an excellent correlation between I_S/I_V and S_{surf}, which suggests that surface modes are related to available surface sites to interact with target gas specimens. Therefore, it should be corroborated from the behavior of the sensor response versus I_S/I_V.

With this aim, the values of sensor response of SnO_2 thick films toward N_2 and gas mixtures 900 ppm CO/N_2 and 90 ppm NO_2/N_2 have been measured and collected in Table 4. The measurement temperatures (380 °C for CO detection and 200 °C for NO_2 detection) were chosen from previous results.[22−24] The electrical response value toward CO $S(CO)$ exceeds the corresponding values measured toward pure nitrogen at 380 °C $S(N_2)$.

Figure 10 presents the $S(CO)$ value as a function of SnO_2 crystallite size (a), specific surface area (b), and Raman parameter I_S/I_V (c) for g, k, and h series. One can observe a general trend of the sensor response diminution as the SnO_2 crystallite size increases. The g, k, and h samples with d_{XRD} = 3−5 nm (prepared at 300 °C) are characterized by a similar sensor response value toward CO. However, for the larger crystallite size $d_{XRD} > 6$ nm, the series prepared by different routes display a different $S(CO) - d_{XRD}$ behavior (Figure 10a). So, it is necessary to conclude that crystallite size value estimated from XRD spectra is not ever the more adequate parameter to predict the gas sensing properties. On the contrary, the dependency on S_{surf} value appears to be more informative to characterize gas sensor properties of these tin oxide samples. All results independently on synthesis method

(20) Pagnier, T.; Boulova, M.; Galerie, A.; Gaskov, A.; Lucazeau, G. *Sens. Actuators, B* **2000**, *71*, 134−139.
(21) Pagnier, T.; Boulova, M.; Galerie, A.; Gaskov, A.; Lucazeau, G. *J. Solid State Chem.* **1999**, *143*, 86−94.
(22) Safonova, O. V.; Rumyantseva, M. N.; Kozlov, R. I.; Labeau, M.; Delabouglise, G.; Ryabova, L. I.; Gaskov, A. M. *Mater. Sci. Eng., B* **2000**, *77*, 159−166.
(23) Safonova, O. V.; Delabouglise, G.; Chenevier, B.; Gaskov, A. M.; Labeau, M. *Mater. Sci. Eng., C* **2002**, *21*, 105−111.
(24) Safonova, O.; Bezverkhy, I.; Fabritchny, P.; Rumyantseva, M.; Gaskov, A. *J. Mater. Chem.* **2002**, *12*, 1174−1178.

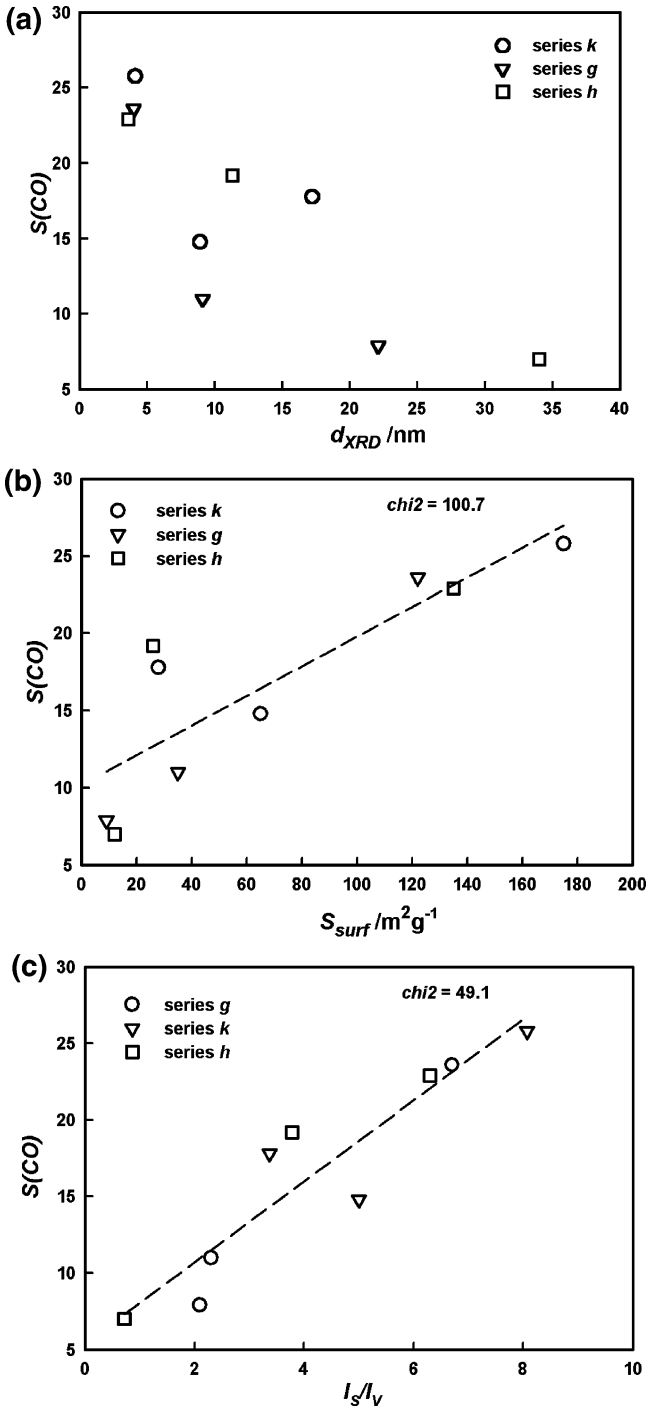

Figure 10. Sensing properties toward CO S(CO) vs SnO_2 crystallite size d_{XRD} (a), specific surface area S_{surf} (b), and Raman parameter I_S/I_V (c).

can be presented as a linear function $S(CO) - S_{surf}$ taking even into account the accuracy of specific surface area and sensor response measurements (Figure 10b). Surprisingly, a better linear correlation is obtained plotting the sensor response against the Raman parameter I_S/I_V than with the specific surface area (Figure 10c). It confirms the usefulness of Raman spectroscopy for the characterization of nanocrystalline tin oxide interactions with gases. Moreover, it has to be pointed out that the specific surface area was measured on powders and not on thick films, while Raman spectra were taken on both, powders and films. Figure 11 shows the changes that are observed for the Raman spectra taken on powders or on films. It corroborates that the film

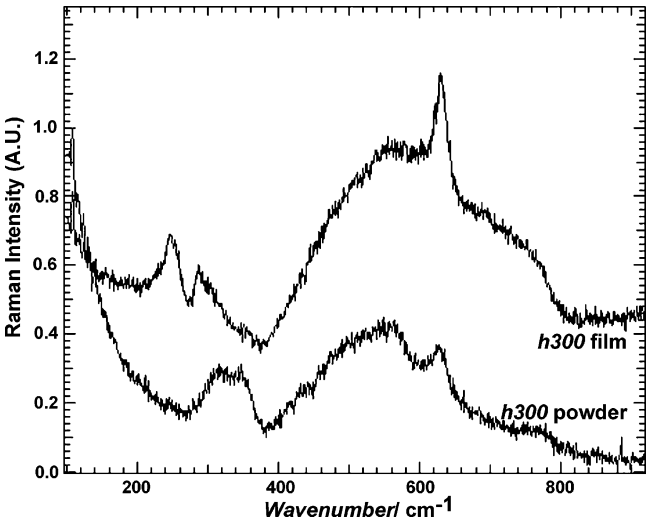

Figure 11. Raman spectra of h300 powders and thick films.

processing has some influence on the nanostructure of the materials, especially on the surface modes, likely due to the 500 °C during 6 h applied treatment to remove the organic solvent used for the paste preparation.

Another important conclusion, which can be drawn from this strong correlation between S(CO) and I_S/I_V, is that the surface modes (I_S) are straightforward connected with the outer layers of the grain, which, according to these results, depend on the synthesis processes. Moreover, these outer layers are modified due to the interaction with the atmosphere.

The sensor response toward NO_2 $S(NO_2)$ of all series is plotted versus d_{XRD} (Figure 12a), S_{surf} (Figure 12b), and d_{BET} (Figure 12c). It is found that behavior of k samples toward NO_2 molecules is different from that shown by the other series. The peculiarity of the encircled points in Figure 12 will be discussed below. The g, h, and s series show the common relationships between sensor response and microstructure parameters: $S(NO_2)$ increases as d_{XRD} values rise too and S_{surf} diminishes. But, even for these series, there is no any common monotonic function applicable to a full set of obtained results.

The examination of nanostructure influence on the sensor parameters of SnO_2 exhibits the opposite trends for detection of reducing CO and oxidizing NO_2 molecules. The S(CO) increases with the specific surface area growth, and vice versa, $S(NO_2)$ increases as the specific surface area diminishes. These results correlate well with data[6] and can be explained from the mechanism of CO and NO_2 detection, which have recently analyzed in the literature from the point of view of the adsorption kinetics[25] or from the temperature treatment influence.[26] So, in the same conditions, materials with higher effective surface area offer for CO gas molecules a higher probability of interaction with adsorbed oxygen and hence they are able to have a higher electrical conductivity change via reaction 1. Moreover, the excellent correlation

$$CO + O_{surf}^{2-} = CO_2 + 2e \qquad (1)$$

with the Raman surface mode intensity also reveals the

(25) Starke, T.; Coles, G. *IEEE Sens. J.* **2003**, *3*, 447−453.

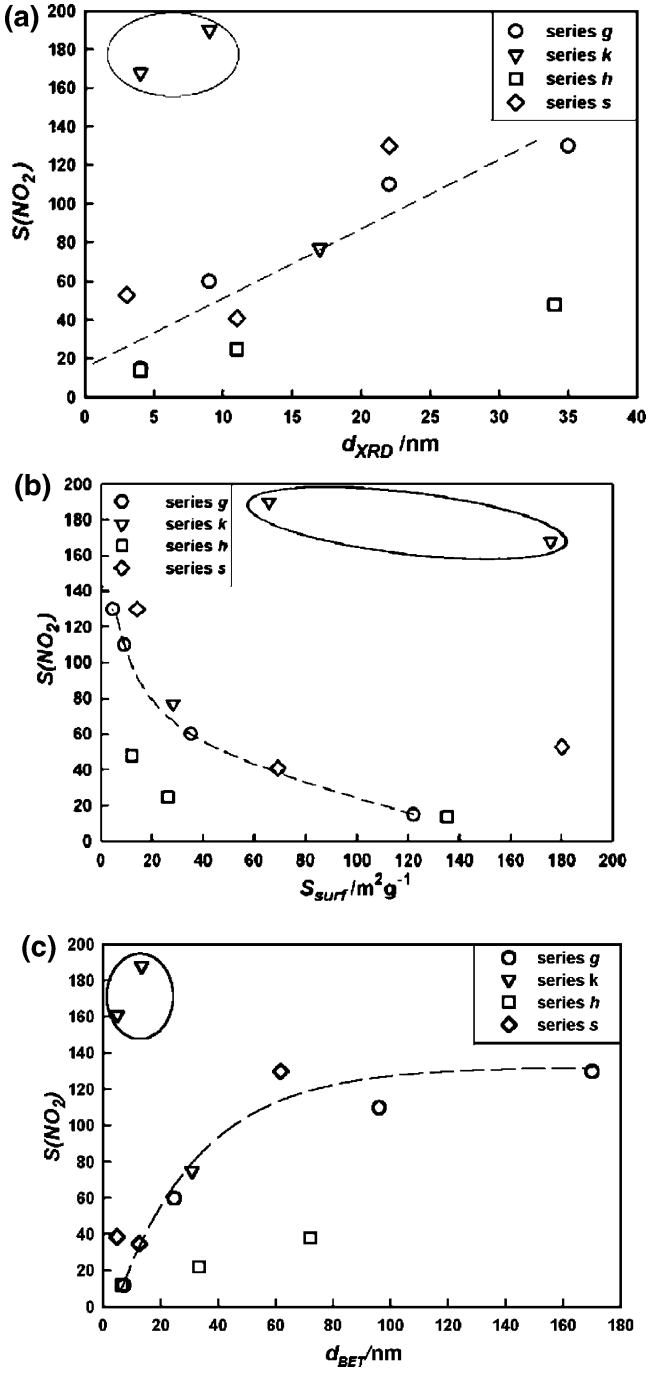

Figure 12. Sensor response toward NO_2 $S(NO_2)$ vs SnO_2 crystallite size d_{XRD} (a), specific surface area S_{surf} (b), and agglomerate size d_{BET} (c).

existence of a relationship between these modes and the density of the available oxygen adsorption sites.

On the contrary, the situation concerning NO_2 sensing mechanisms is quite different. In general, the density of adsorbed nitrate groups is influenced, on one hand, by the concentration of available electrons to form and absorb the NO_2^- group and, on the other hand, by the amount of available adsorption sites at the grain surface that can be altered by the competition with the oxygen. For example, a nanograin surface that is highly covered by adsorbed oxygen—see the high intensity of the Raman surface modes

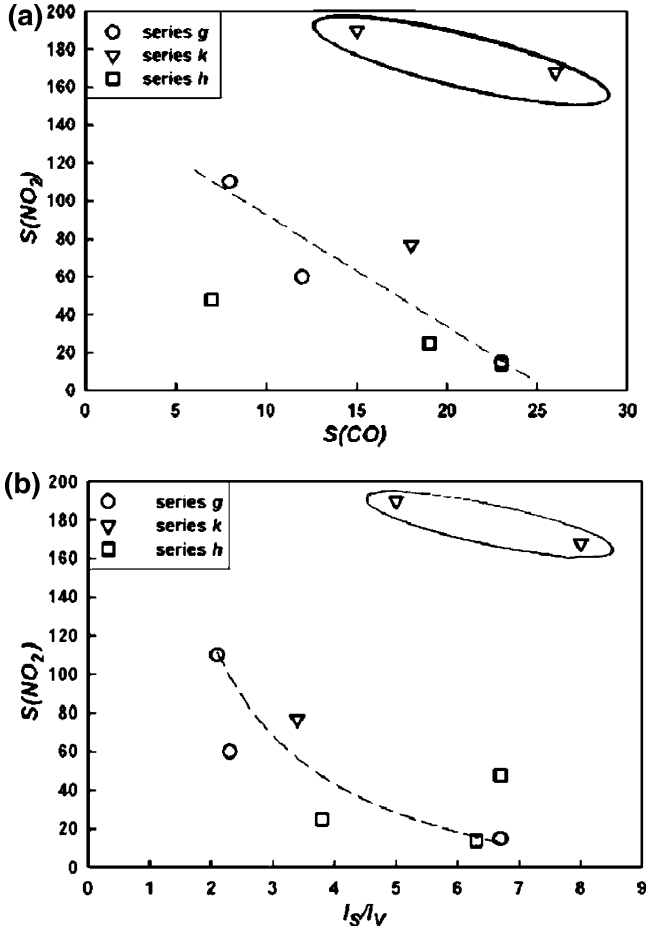

Figure 13. Sensor response toward NO_2 $S(NO_2)$ vs sensor response toward CO $S(CO)$ (a) and Raman parameter I_S/I_V (b).

according to the data given in Figure 10c—has already a high density of negative charge that can prevent or render more difficult any action for increasing the surface negative charge such as is required by the NO_2 molecule adsorption.

Therefore, the existence of an inverse correlation is quite plausible between the sensor responses for CO and NO_2, except for some cases that will be discussed below (Figure 13a). So, experimental results seem to corroborate that for high I_S/I_V values the sensor response to NO_2 is low and it increases when the surfaces modes diminish (Figure 13b) in agreement with the previous arguments. Moreover, it is again proved that there is a better correlation between the sensor response for NO_2 and the active surface (Figure 12b) than if it is considered against the grain size, d_{XRD} (Figure 12a).

These results agree with the model for explaining the influence of heat treatment on the material sensitivity to NO_2 as supposed in ref 6. Apparently, the thermal treatment procedure gives rise to surface modification, which is revealed by the diminution of the surface disorder or by the faceting of the grains. Both mechanisms decrease the oxygen adsorption sites in comparison with the case of small nanograin without or with low-temperature treatments and it facilitates the availability of electrons and specific sites for NO_2 adsorption. A similar situation occurs due to the material grinding process what modifies the surface. Then, after annealing at high temperature, 700−1000 °C, the sensor response to NO_2 is also improved.[6]

(26) Cha, G.; Bui, A.; Baek, W.; Lee, S.; Huh, J. *Met. Mater. Int.* **2004**, *10*, 149−152

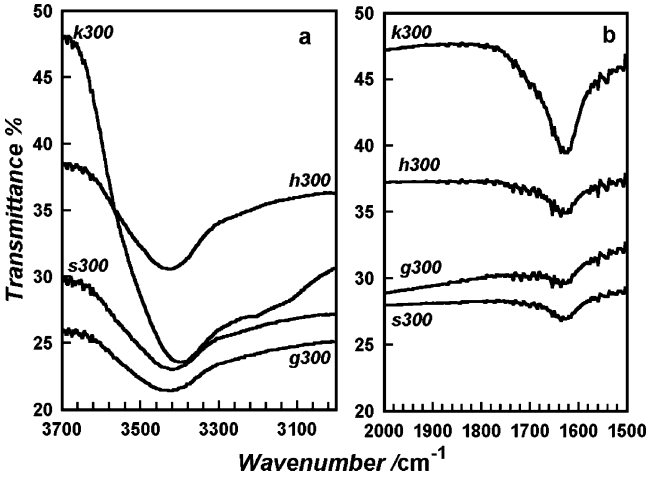

Figure 14. FTIR spectra of different SnO_2 samples calcined at 300 °C.

The peculiarities of the encircled points in Figures 12 and 13 can be derived from different compositions of corresponding samples. The samples k300 and k500 (encircled points) are characterized by maximum mass loss (TGA), which can be attributed mainly to water elimination. The first step of weight loss is a conversion of water to surface OH groups.[27] For this reason, the presence of OH groups was checked by FTIR spectroscopy. Figure 14 shows the FTIR spectra taken with KBr (2 mg of SnO_2 per 200 mg of KBr), corresponding to the samples g300, k300, h300, and s300. The spectra exhibit a broad band around 3450 cm^{-1} in the νOH vibration range (Figure 14a) and an intensive band close to 1640 cm^{-1} (Figure 14b) associated with the presence of adsorbed water. The comparison of band intensities indicates that k300 contains much more OH groups than other samples. It is known that surface OH groups play an electron donor role.[30] This situation enhances the probability of capturing one electron by NO_2, and, hence, under this situation, it increases the sensor response. It is clear and accepted that OH groups play an important role in sensor characteristics,[31] but a detailed analysis of it is a matter for other specific analysis rather related to the origin of the other Raman bands found below 400 cm^{-1}. However, it is out of the scope of this work. The samples k300 and k700 also stand out because of their higher Cl content (Table 1) that could also suggest a combined effect with the excess of the OH groups in these samples.

Conclusions

SnO_2 nanocrystalline powders with the grain size of 3−36 nm and specific surface area up to 180 $m^2\ g^{-1}$ have been prepared by four different routes of wet chemical synthesis. High-resolution TEM and electron diffraction experiments have shown that SnO_2 powders were composed of nanocrystals with distorted rutile structure. Crystallite size was derived from X-ray diffraction and HRTEM, which also provided a size distribution of the particles. The influence on the intensity of Raman surface vibration modes of the calcination temperature, crystallite size, and specific surface area has been studied and an excellent correlation was found between the Raman surface vibration mode intensity and the active surface. It has been considered to corroborate that the Raman surface vibration modes reveal the availability of active surface sites for interaction with the target gas. It has been corroborated from the sensor response of corresponding thick films which has been measured toward reducing CO and oxidizing NO_2 molecules in N_2-based gas mixtures. The nanostructure influence on the sensor parameters exhibits opposite tendencies for CO and NO_2 detection. High specific surface area/Raman surface vibration mode intensity increases the sensor response value for CO and reduces the detection for NO_2. It was found that the intensity of Raman parameter I_S/I_V shows the best linear correlation with gas response of materials to CO. The better correlation than that with specific surface area is explained by the fact that Raman spectra were taken from finished sensors, while specific surface area was measured on as-obtained powders. Adsorbed species such as OH groups and Cl originating from the synthesis procedure seem to also present a significant impact on sensor properties.

Acknowledgment. This work was supported by INTAS grant N2000-0066 and RFBR grants N01-03-32728 and N03-03-32586. The authors are grateful to Dr. Jordi Arbiol (EME and SCT of the University of Barcelona) for the TEM investigations.

CM0490470

(27) Lenaerts, S.; Roggen, J.; Maes, G. *Spectrochim. Acta, A* **1995**, *51*, 883−894.
(28) Chiorino, A.; Ghiotti, G.; Prinetto, F.; Carotta, M. C.; Martinelli, G.; Merli, M. *Sens. Actuators, B* **1997**, *44*, 474−482.
(29) Leblanc, E.; Perier-Camby, L.; Thomas, J.; Gibert, R.; Primet, M.; Celiu, P. *Sens. Actuators, B* **2000**, *62*, 67−72.
(30) Bârsan, N.; Weimar, U. *J. Electroceram.* **2001**, *7*, 143−167.
(31) Ribeiro, S.; Santilli, C.; Pulcinelli, S.; Fortes, F.; De Oliveira, L. *J. Sol−Gel Sci., Technol.* **1994**, *2*, 263−267